Different Tracers Give Different Gravitational Mass Distributions

Dalia Chakrabarty[1]

School of Physics & Astronomy, University of Nottingham, Nottingham NG7 2RD, U.K. e-mail:
dalia.chakrabarty@nottingham.ac.uk

June 29, 2009

ABSTRACT

Context. Charting the extent and amount of dark matter (DM) in the Universe is highly appealing but is equally hard since it is only through the interpretation of its effect that we can track the DM distribution. Given the implementational problems, it is non-trivial to quantify the effects of DM on the motion of individual test particles in an elliptical galaxy, with the aim of identifying its total gravitational (i.e. luminous+dark) mass distribution; expectedly, this has caused controversy.

Aims. Leaving such technical details aside, in this article we report on the danger of the very notion that test particle velocities can reliably imply total mass distribution in galaxies.

Methods. We expose the fallibility of this mass determination route, by undertaking a Bayesian analysis of the observed line-of-sight velocities of individual test particles belonging two distinct types: planetary nebulae (PNe) and globular clusters (GCs) that span the outskirts of the galaxy NGC 3379.

Results. The PNe and GC data are shown to be drawn from independent phase space distributions and total mass density distributions that are derived from implementations of the two kinematic data sets are found to be significantly different, leading to significant (at 1-σ level) differences in the resulting enclosed mass profiles. The assumption of isotropy in phase space is tested with a robust Bayesian test of hypothesis; the GC velocities are found to be much more supportive of the assumption of isotropy than are the PNe data. We find that this recovered difference in the state of isotropy between the phase space distributions that the data are drawn from, cannot be used to reconcile the differences in the recovered mass density distributions.

Conclusions. The recovered dichotomy is indicative of the risk involved in the interpretation of mass distribution obtained from tracer kinematics, as the galactic mass distribution.

Key words. Galaxies: kinematics and dynamics; individual: NGC 3379; Methods: statistical

1. Introduction

NGC 3379, or M 105, seems to have initiated its journey within the observational domain, in neglect - though Pierre Mechain is credited with its discovery in 1781, it did not initially make it to Messier's catalogue. Amends were made later in 1947, when it was among four new objects that were "added to the accepted list of Messier's catalogue as nos. 104, 105, 106 and 107" (from Helen Sawyer, 1947). In spite of this early inattention, NGC 3379 has recently been in vogue. Romanowsky et. al (2003) had advanced the idea that this system is one of the five "naked galaxies", the mass distributions of which were tracked with the Planetary Nebula Spectrograph (PNS). Such claims were contested by Dekel et. al (2005), though Douglas et. al (2007) defend the earlier result of Romanowsky et. al (2003) by analysing the kinematic data of 214 planetary nebulae (PNe) in NGC 3379.

Dekel et. al (2005) advance the possibility that NGC 3379 might in actuality be a triaxial system and that it is this intrinsic asphericity that causes the measured line-of-sight projected velocity dispersion (σ_p) to appear less than what it is, for certain inclinations. However, Douglas et. al (2007) argue that such a geometric reasoning, though possible, is unlikely to be a plausible explanation for the other three naked galaxies that were reported by Romanowsky et. al (2003). Additionally, the suggestion that it is the idiosyncracy of this system that the detected PNe data might be tracing a sample of younger stars, rather than the stellar population as a whole, was judged implausible by Douglas

et. al (2007) based on the rarity of such an occurrence within a single system, with the sole identification of the presence of multiple PN populations in NGC 4697 (Sambhus, Gerhard & Méndez 2006; Sambhus et al. 2005).

However, the most pressing concern of Dekel et. al (2005) is the possibility that radial anisotropy might be introduced as a result of a merger; Douglas et. al (2007) disagree that this could explain the identification of the low dark matter content in NGC 3379, given that the existence of anisotropy was included in the data-fitting process employed in Romanowsky et. al (2003). They stress that the anisotropy profile recovered from the PNS data and that obtained from the simulations presented in Dekel et. al (2005), are similar in nature.

Similar concerns about the mass-anisotropy degeneracy have repeatedly been voiced by various workers in the field of mass estimation from tracer kinematics (Łokas & Mamon 2003; Koopmans 2006; Côté et al. 2001, 2003). The relevant question to ask would be: is the uncertainty in mass estimates, implied by our lack of information about the prevalence of anisotropy, so large that we cannot conclude anything significant about the mass distribution in the system? If the response is in the affirmative, then of course it is futile to seek a solution for the mass density from tracer kinematics. Recovering the host galaxy mass distribution, while incorporating full-fledged anisotropy, requires the tracer kinematic sample size to exceed typical numbers - in fact, the sample of 214 planetary velocities that is available for NGC 3379, represents one of the relatively larger samples available. If on the other hand, our analysis can - based upon the limited measurements and the assumptions invoked to tackle

the lack of anisotropy estimates - allow us to infer usable information about the mass distribution of the system, then it still makes sense to undertake such analysis. Of course, such inferred mass distributions will have to be qualified adequately, in light of the relevant assumptions.

In this contribution, we report on an investigation of the validity of the usage of tracer kinematics in the determination of the mass of the host galaxy. This is done in reference to the elliptical galaxy NGC 3379, which is the only elliptical galaxy yet, for which kinematic information is available for individual members of two tracer samples that pertain to two separate classes (PNe and GCs), over an extensive radial range spanning the outer parts of the galaxy (radius $\gtrsim 5R_E$). The analysis is performed with the Bayesian algorithm CHASSIS under the assumptions of spherical geometry and the necessary assumption of phase space isotropy (given the small GC data sample); relaxation of the latter assumption is being explored currently (Chakrabarty & Saha, in preparation). CHASSIS has been calibrated against N-body descriptions of star clusters (Chakrabarty & Portegies Zwart 2005) and has been applied to gauge the total mass density distributions in various systems (Chakrabarty & Saha 2001; Chakrabarty 2006; Chakrabarty & Raychowdhury 2008).

The basic motivation behind our work is to check the effect of distinct tracer kinematic data in determining the mass distribution of a given galactic system. If the data sets imply different σ_p profiles, we can infer that the data are drawn from distinct phase space distributions. However, we expect that a unique potential of the galaxy must be arrived at, irrespective of the kinematic data that is input into the used mass determination scheme. Consequently, if we obtain different mass profiles with two different data sets, we would feel alarmed and question the compatibility of each data set with the assumptions inherent to the used scheme. The aim for such an exercise is to ascertain if the differences between the derived mass profiles can be reconciled by invoking the discord between the assumptions and the data. In case such reconciliation is not possible, we will use the results to argue for caution against galactic mass distributions obtained from tracer kinematics.

On the other hand, the structure of the conventionally used Jeans Equation formalism does not suggest any a-priori reasons for anticipating the recovery of a unique enclosed mass distribution from the implementation of distinct σ_p and number density (ν) distributions unless a conspiracy exists between the gradients of the σ_p and ν, to always yield the same mass distribution. Similarly, if any operational mass determination scheme implies different mass distributions with distinct kinematic data, it is not altogether surprising.

The input data used in the work include LOS velocities of 164 planetaries (PNe) from the PNS survey (Douglas et. al 2007) and of 29 globular clusters (GC) that were reported by (Bergond et. al 2006). Given that an assumption of isotropy is questionable, Bayesian significance testing of the goodness of this assumption will be undertaken for each data input.

2. CHASSIS

CHASSIS is a Bayesian non-parametric algorithm that uses MCMC optimisation to recover the total gravitational potential Φ and the phase space distribution function f of a host system, by analysing a sample of one or more components of the velocity vector of tracers that reside in this host. Actually, Φ is calculated at each iterative step from the total mass density ρ using Poisson equation. We assume a *spherical geometry* and *isotropy in velocity space*: $\rho = \rho(r)$ and $f = f(E)$ where r is the

spherical radius and E the energy. We are basically looking for $\Pr(f(E), \rho(r)|data)$ and estimate this using Bayes theorem - the $\{f, \rho\}$ pair that gives the highest posterior probability is sought. However, in this search for the most likely configuration, we do not have any prior notions about $f(E)$ or $\rho(r)$, except that we require:

$$f(E) \geq 0, \quad \text{and} \quad \rho(r) \geq 0,$$
$$\frac{df(E)}{dE} < 0 \quad \text{and} \quad \frac{d\rho}{dr} < 0. \tag{1}$$

Other than such monotonicity & positivity conditions, the sought functions are retained as completely free-form. In fact, $\rho(r)$ and $f(E)$ are represented by constructions that are each akin to one dimensional bar-graphs or the $\rho - histogram$ and $f - histogram$; the radial range is binned and density is held a constant in each radial bin, during any step. Similarly f is a constant over any energy bin.

The algorithm starts with seeds for the f and ρ and at the beginning of each step, the f and ρ histograms are tweaked slightly over their past form, in scale and shape. This process repeats itself till the likelihood of the data having been drawn from the current f, at the current potential, is detected to be the maximum, by the optimiser which is the Metropolis-Hastings algorithm (Hastings 1970). The recovered $f(E)$ and $\rho(r)$ are ascribed ± 1-σ error bars that describe the ± 1-σ extent of the wandering within the neighbourhood of the global maxima in the likelihood function. The observed error bars in velocity are convolved in, assuming a Gaussian error distribution for the observed errors.

The quantities that are directly recovered from the algorithm are used to generate other physically interesting distributions, such as the enclosed mass and velocity dispersion profiles.

Now, as was discussed in Chakrabarty & Portegies Zwart (2005), CHASSIS bears the peculiarity that an erroneous assumption of velocity isotropy, over a radial range where anisotropy actually prevails, results in the over-estimation of mass. This can be qualitatively understood as the following. When sphericity is mistakenly assumed in a 3-D spatial volume in a massive system that is actually eccentric, then at any radius r, the enclosed mass is over-estimated, i.e. the local value of the integral of the space density over all volume is over-estimated. Similarly, when isotropy is mistakenly assumed in velocity space where anisotropy reigns, the integral of the velocity space density, over all velocities, is over-estimated. But the latter is the integral that is proportional to the number density. Hence, CHASSIS over-estimates the number density at those radii where anisotropy prevails. It is expected that mass density does not decrease with number density ν; so our misrepresenting anisotropy, in general, implies over-estimation of the mass density (empirically verified in Chakrabarty et. al 2009, in preparation).

2.1. Justifying Choice of Assumption of Isotropy

Here we discuss the motivation behind choosing to work with the assumption of phase space isotropy, i.e. assume $f = f(E)$ rather than have a simple anisotropic representation such as a 2-integral f. From experiments with a 2-integral f that are currently underway, (Chakrabarty & Saha, 2009), it appears that for sample sizes $\lesssim 200$, the recovered ρ is marked by very large error bars, by which is implied uncertainties high enough to render the recovered $\rho(r)$ meaningless. Given that the aim of the current work is to compare the effects of the PNe and GC data - where the GC sample has only 30 data points in it - the choice of an

anisotropic f is therefore pointless. Rather, *we find it useful to work with the isotropy-assuming CHASSIS and then undertake a robust statistical test of hypothesis to check if our recovered $\rho(r)$ is biased in the available data.*

3. Results

Runs were conducted with different initial seeds for the density and the f, to check for robustness of the answers to seed selection.

3.1. Seeds

In order to establish the independence of the recovered results from the initial choice of the seed ρ and f, we have performed multiple runs beginning with distinct seed characteristics. The general form of the seed density $\rho_{seed}(r)$ has been chosen to be:

$$\rho_{seed}(r) = \frac{\rho_0}{\left(\dfrac{r}{r_c}\right)^{\alpha_1}\left(1+\dfrac{r}{r_c}\right)^{\alpha_2}}, \qquad (2)$$

where ρ_0 is the amplitude determining parameter and α_1, α_2 and r_c affect the shape of the seed density profile. Of these, we find CHASSIS totally unaffected by the choice of ρ_0; convergence is achieved with the other parameters lying in moderately extensive ranges. Such ranges are reflected in the different seeds that we work with (see below).

The seed $f_{seed}(E)$ (where E is energy, with $-1 \leq E \leq 0$), is chosen to be either power-law in form (with the power β) or exponential:

$$\begin{aligned}f_{seed}(E) &= \exp^{-E} \text{ or} \\ &= (-E)^\beta\end{aligned} \qquad (3)$$

Three different runs performed with the PNe are characterised by seeds that are described as follows.

- PNe-RUN I: r_c=30kpc, α_1=2.8, α_2=1, $f_{seed} = \exp^{-E}$.
- PNe-RUN II: r_c=20kpc, α_1=3.8, α_2=2, $f_{seed} = (-E)^3$.
- PNe-RUN III: r_c=10kpc, α_1=1.8, α_2=3, $f_{seed} = (-E)^5$.

Three different runs performed with the GCs are characterised by the following seeds.

- GC-RUN I: r_c=30kpc, α_1=2.8, α_2=1, $f_{seed} = \exp^{-E}$.
- GC-RUN II: r_c=5kpc, α_1=3.6, α_2=2, $f_{seed} = (-E)^5$.
- GC-RUN III: r_c=10kpc, α_1=3.2, α_2=3, $f_{seed} = (-E)^2$.

The 3D mass density profiles that are recovered from the three PNe and GC runs are shown in the panels of Figure 1. The overlapping of the density distributions recovered from these assorted runs implies that the obtained results are independent of the initial guess for the density and f. The recovered density profiles bear different degrees of uncertainty depending on the data sizes implemented in the particular run and to a smaller extent, on values to which the different knobs inside our MCMC optimiser are set (for example, the details of the jump probability distribution and the acceptance probability threshold or temperature).

Figure 1 also presents the phase space distribution functions, approximated as isotropic, as recovered from two different runs of CHASSIS, each performed with the kinematic data of a distinct type of mass tracer.

3.2. Recovered ρ and f; derived distributions

Given the similarity of the recovered density distribution from different runs performed with a given tracer data, results from a sample PNe run (PNe-RUN I) are compared to those from GC-RUN I. This is shown in Figure 2; it includes comparison between the recovered total mass density $\rho(r)$, enclosed mass $M(r)$, total cumulative mass to light ratio in the B-band $\Upsilon_B(< r)$ and the circular velocity defined by $v_c = \sqrt{GM(r)/r}$.

From the recovered $\rho(r)$, $M(r)$ is estimated. $\rho(r)$ recovered from PNe-RUN I drops much quicker than that from GC-RUN I. This is further reflected in the enclosed mass profile $M(r)$, which flattens out in the result from PNe-RUN I by about 7 kpc, while continuing to rise even at 25 kpc, in GC-RUN I.

Now, a flat or constant enclosed mass profile would imply that the quantity defined as akin to the circular velocity ($v_c = \sqrt{GM(r)/r}$), would be falling simply as $r^{-1/2}$, i.e. as in a Keplerian potential. Here G is Newton's Universal Gravitational constant. This quantity is shown in the lower right panel of Figure 2, on which is over-plotted the true Keplerian $r^{-1/2}$ function, normalised by G times the mass that is recovered at $r=3R_E$, from PNe-RUN I. As is evident from the figure, the true Keplerian fall-off and the v_c estimated from PNe-RUN I overlap very well, though $v_c(r)$ recovered from GC-RUN I is much flatter than the $r^{-1/2}$ fall-off. This is only another way of expressing the fact that $M(r)$ flattens out to a constant mass for PNe-RUN I while it continually rises for GC-RUN I.

3.3. Recovered LOS velocity dispersion

Figure 3 represents the LOS velocity dispersion distributions $\sigma_p(r)$ that are recovered from PNe-RUN I and GC-RUN I. The recovered f is used, in conjunction with the derived ρ, to calculate $\sigma_p(r)$. Again, we notice the significantly flatter shape of the $\sigma_p(r)$ distribution that is obtained from GC-RUN I, as distinct from the steeply falling trend in the distribution estimated from the PNe-RUN I.

It is not surprising that CHASSIS identifies distinct $\sigma_p(r)$ profiles from the implementation of the 2 different kinematic samples. After all, such distinct kinematic data sets would result in the construction of the distinct $\sigma_p(r)$ profiles (which in turn imply distinct phase space density distributions).

3.4. Photometry used for Υ_B estimation

The cumulative Υ profile, in the B-band is shown in Figure 2. The calculation of $\Upsilon(< r)$ of the galaxy requires knowledge of photometry. The surface brightness distribution is the same as used in Douglas et. al (2007) and has been kindly provided by Aaron Romanowsky. It is deprojected in the spherical geometry, using the non-parametric deprojection code DOPING (Chakrabarty & Ferraese 2008), to give us the luminosity density distribution $j(r)$ (see Figure 4). Though DOPING can perform deprojection in general triaxial geometries, here we limit ourselves to deprojection under sphericity, since CHASSIS assumes sphericity (and velocity isotropy). In fact, the photometric data used to calculate $j(r)$ in Douglas et. al (2007) were analysed under sphericity too; the deprojection there was performed by fitting analytical distributions to the data. Figure 4 shows the analytical 3-D luminosity density distribution obtained by the fitting method of Douglas et. al (2007), as compared to the $j(r)$ we recover with DOPING. The luminosity density distributions compare well with each other, though, as expected, the $j(r)$ obtained by Douglas et. al (2007) from fitting is smoother - the un-
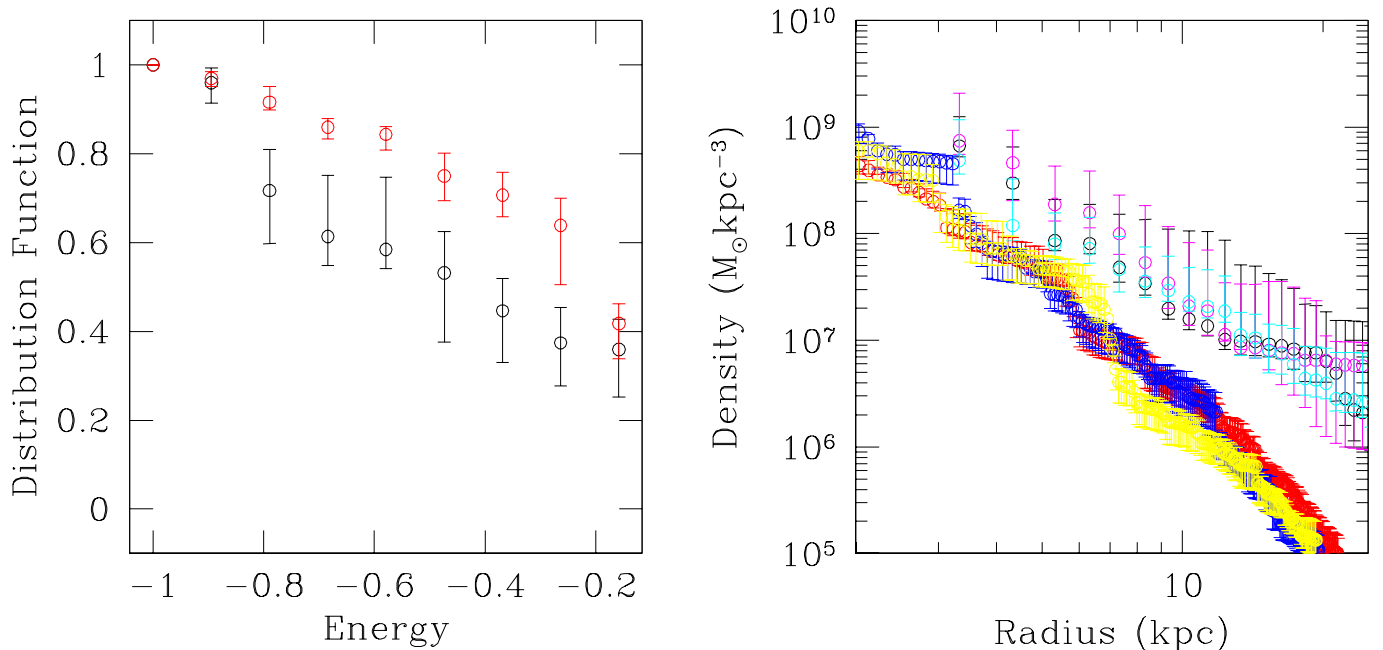
Fig. 1. Right panel: density profiles recovered from the 3 PNe runs and the 3 GC runs. The results of the PNe runs are shown in red, yellow and blue while the density distributions obtained by using the GC kinematics are in black, magenta and cyan. As is apparent from the figure, starting with different seeds results in density profiles that are consistent with each other, as long as the same kinematic tracer sample is used in the analysis. Left panel: isotropic (normalised) phase space distribution functions recovered from PNe-RUN I (in red) and from GC-RUN I (in black). The distribution function is plotted as function of energy.
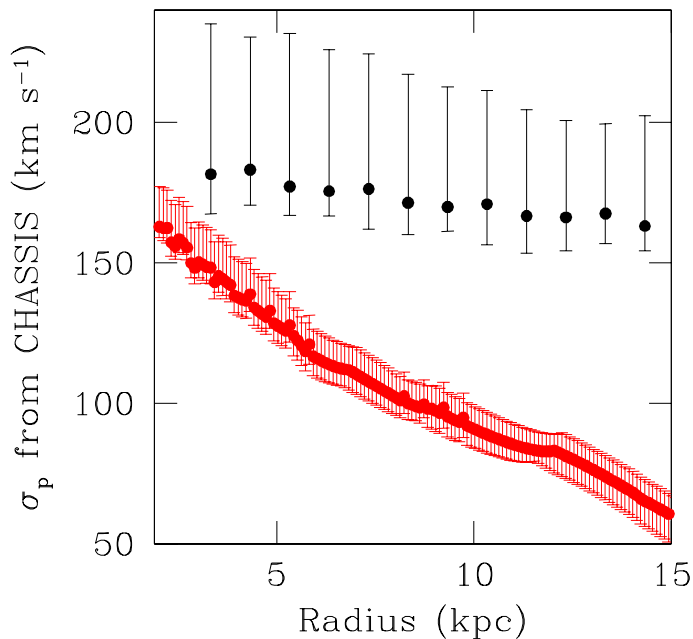
Fig. 3. The LOS velocity dispersion profiles recovered from PNe-RUN I (in red) and from GC-RUN I (in black).

dulations in the observed surface brightness is better represented by our recovered $j(r)$.

Our deprojected $j(r)$ is used to calculate the cumulative light distribution, which when compared to $M(r)$, gives us the cumulative mass-to-light ratio $\Upsilon(< r)$. Our results indicate that the mass to light ratios of the outer parts of NGC 3379, as tracked by the PNe velocities is significantly depressed in amplitude compared to that implied by the GC kinematics! Individual consideration of the PNe analysis leads to a "naked" interpretation for

NGC 3379, in line with what was suggested by Douglas et. al (2007) and Romanowsky et. al (2003). The GCs on the other hand, paint a diametrically opposite picture of the galaxy in terms of DM content - in fact, we find the mass-to-light ratios in B to be high enough to suggest that the galaxy is rich in DM, in line with Bergond et. al (2006).

The $\Upsilon(< r)$ recovered from the PNe-RUN, at $5R_E$ lies between 10 and 20. This is slightly higher than what Douglas et. al (2007) advance for NGC 3379, in spite of both mass-to-light calculations having used concurrent luminosity density distributions (see Figure 4). This slight discrepancy is attributed to the assumption of isotropy in our work which artificially augments mass density values wherever anisotropy exists.

Of course, this apparently dichotomous view of the potential of a given galaxy is not acceptable; this triggers careful examination of the assumptions involved, the principle among which is that of isotropy.

4. Testing for isotropy

The test for the validity of the assumption of isotropy, given the observed data, is an exercise in statistical hypothesis testing. Such test of significance will not *prove* or *disprove* the isotropic nature of phase space of NGC 3379 but will provide a probabilistic estimate of the goodness of the assumption of isotropy in the data. A *proof* of $f = f(E)$ is only possible if CHASSIS incorporates the full anisotropy - a simple way to do so is to consider a 2-integral f, such as $f = f(E, L)$ where L is the angular momentum. Such a scheme will however yield density profiles marked by unacceptably large uncertainties unless the input kinematic sample is sufficiently high (see Section 2.1). Given this operational difficulty, we settle for isotropy and test for the compatibility of our assumption of isotropy with the measured data, using a robust statistical test.
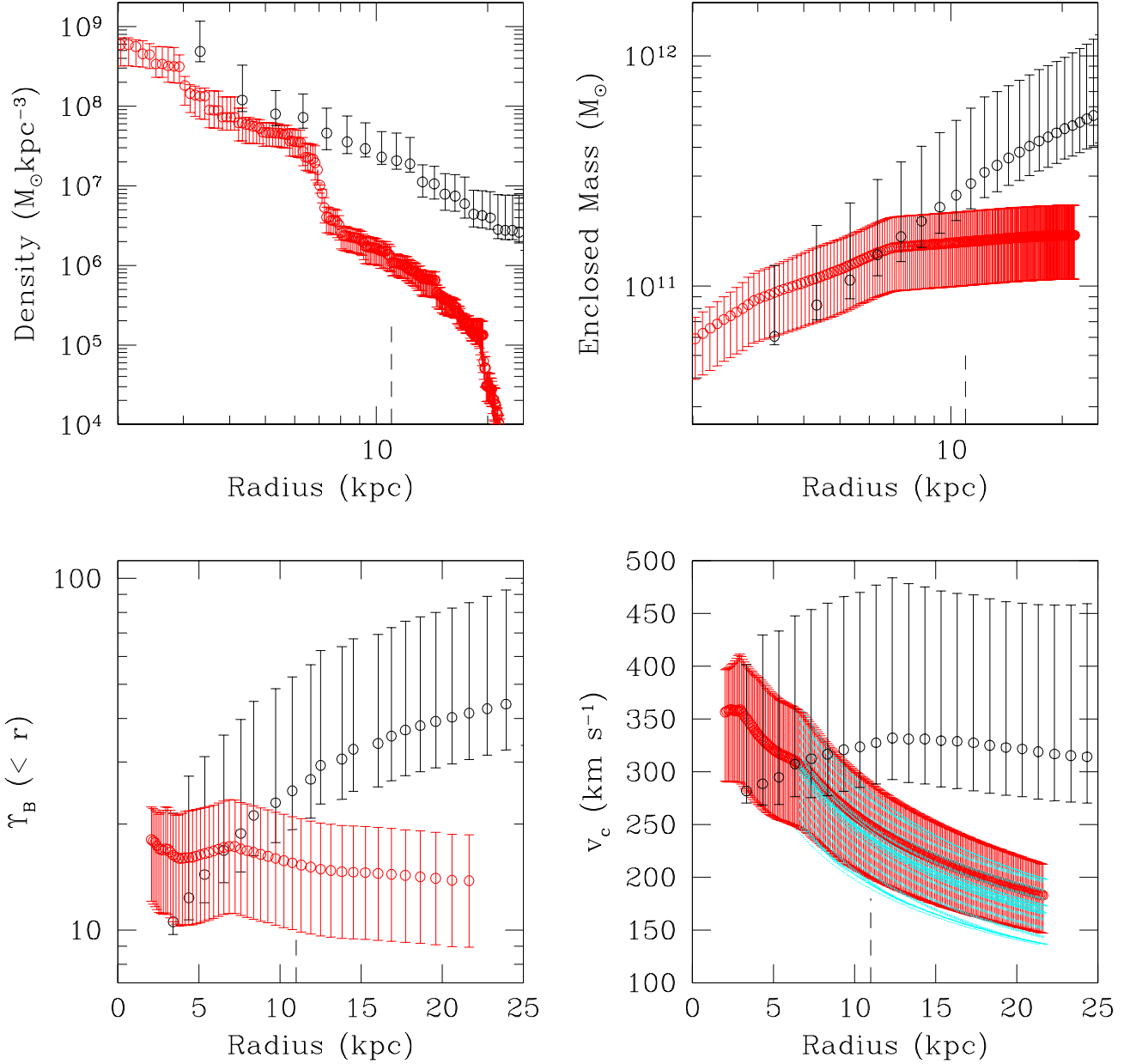
Fig. 2. Top left panel shows the total mass density recovered from PNe-RUN I (in red) and GC-RUN I (in black). The enclosed mass profiles $M(r)$, as extracted from these runs, are represented in the corresponding colours in the top right panel. The lower left panel represents the B-band cumulative mass-to-light profiles $\Upsilon_B(< r)$, estimated from the $M(r)$ recovered from the corresponding run, and the luminosity density shown in Figure 4. The lower right panel shows the radial distribution of the quantity akin to the circular velocity v_c, as obtained from the two runs performed with the two sets of tracers. The points in cyan correspond to the function $r^{-1/2}$, normalised by GM_0, where M_0 is the mass (with errors) found to be enclosed within $3R_E$, from PNe-RUN I.

While traditionally this is typically done by undertaking a calculation of p-values (Kempthorne & Folks 1971), better, more sophisticated techniques also exist, such as the Bayesian evidence measures, a robust example of which is the Fully Bayesian Significance Test or FBST (Pereira & Stern 1999; Pereira, Stern & Wechsler 2008). A highly satisfying aspect of the Bayesian evidence value is that it obeys the Likelihood Principle (Basu 1975; Birnbaum 1962).

p-values provide the probability that the value of the sought measure, given randomly generated data, is at least as inconsistent with the null hypothesis as that corresponding to the observed data is. "Small" p-values imply that the null is unlikely to be true; the definition of "small"ness is traditionally held as 5% significance. Also, the estimation of p-values is an exploration in sample space, while we would prefer to work in parameter space. Most importantly, testing with p-values leads to rejection or non-rejection of the null hypothesis, at the pre-set significance
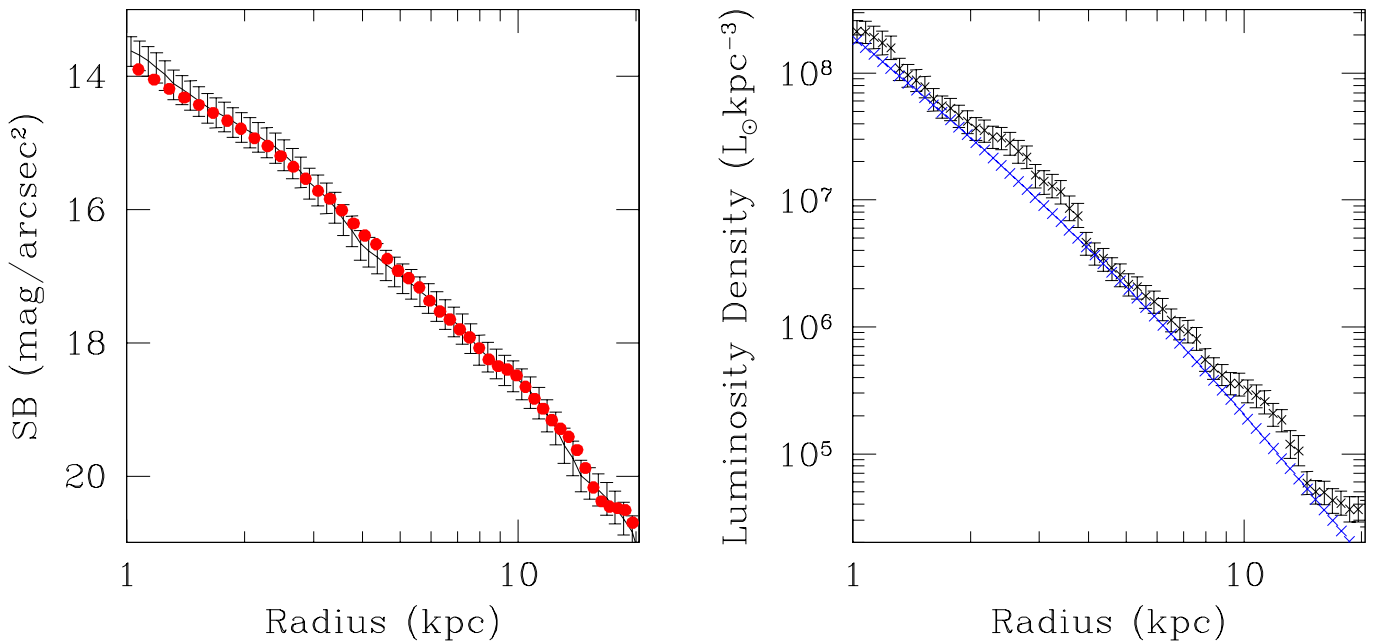
Fig. 4. The points in black in the right panel represent the luminosity density profile ($j(r)$), of NGC 3379, as obtained by deprojecting the surface brightness profile in the *B*-band (shown in red, in the let panel) by the deprojection algorithm DOPING, under an assumption of sphericity. The projection of this deprojected density (in black, in the right panel) is compared to the measured brightness data. The analytical $j(r)$ used by Douglas et. al (2007) is shown in blue in the right panel.

level; the size of the effect cannot be evaluated with *p*-values. *p*-values are indeed mired in a web of problems, including the potential to falsely inflate compatibility with the null. A rather severe criticism is presented by Hubbard & Lindsay (2008).

4.1. General FBST - a brief introduction

Given such shortcomings, FBST is a welcome change. Here we discuss the salient features of the general FBST formalism that tests the null hypothesis that the relevant parameter - θ - has a value of θ_0, i.e. $H_0 : \theta = \theta_0$, (say) where θ is assumed to be distributed continuously in the parameter space Θ. Once the essence of FBST is clarified, we move on to *our* implementation of FBST in a non-parametric context; see Chakrabarty (2009) for greater details.

FBST measures the evidence in favour of H_0 by identifying the most likely, H_0-obeying measure (θ^*) and then quantifies the probability of identifying θ that are more likely than θ^{*}[1]. Such θ comprise the tangential set T. In other words, T is composed of all θ that are more consistent with the observed data ({*data*}) than θ_0 is.

Then the evidence in favour of H_0 is:

$$ev = 1 - \Pr(\theta \in T | \{data\}), \quad \text{where}$$
$$T = \{\theta : \Pr(\theta | \{data\}) > \Pr(\theta^* | H_0)\}. \tag{4}$$

Here the probability of recovering θ, given the measurements {*data*} is $\Pr(\theta|\{data\})$ and θ^* is the point in Θ space, satisfying H_0, that maximises this probability.

Thus, FBST involves identification of θ^*, followed by integration over T.

---

[1] In other words, FBST requires identification of all θ, the posterior probability corresponding to which is in excess of that of θ^*.

4.2. Implementation of FBST

We present below a version of the *ev* calculation, adapted for the case when the measure θ is non-parametrically estimated. This is the first reported implementation of FBST in a non-parametric situation. In this case, the integration of $\Pr(\theta|\{data\})$ over the T is difficult and can be replaced by a case-counting scheme. In our work,

– $\theta \equiv \{\rho - f\}$histogram pairs,
– Θ is the space of all $\{\rho - f\}$histograms,

For us, the null hypothesis is that the data is isotropic, i.e.

$$H_0 : \hat{f} = \Psi[E(\sum_i v_i^2/2 + \Phi(r))], \tag{5}$$

where

– $\hat{f}$ is the phase space density from which the *input* kinematic sample is drawn, and
– Ψ is some function: $\Psi > 0$ for $E < 0$ and $\Psi = 0$ otherwise.

We are not sure if the observed GC and PNe data are drawn from isotropic phase space distributions and so test if H_0 is true.

Our MCMC optimiser, upon convergence, identifies a range of profiles of $\rho(r)$ and $f(E)$, within a ± 1-σ error band. Using this achieved solution, we generate n samples of N_{data}-sized data sets corresponding to the observables, i.e. v_z, x_p, y_p. Here N_{data} is the size of the observed data and v_z is the LOS velocity coordinate while the plane of the sky coordinates are x_p, y_p. Thus, these n generated velocity data sets are drawn from the *isotropic* $f(E)$ recovered by CHASSIS. Let us refer to these generated data sets as $D_{CHASSIS}$. Therefore, kinematic information in $D_{CHASSIS}$ are drawn from a phase space density which is indeed isotropic, unlike the observed data which are not necessarily drawn from an isotropic f.

Next we input each of the n $D_{CHASSIS}$ into CHASSIS, to start n new runs. This generates new sets of $\{\rho - f\}$histograms. H_0 is

obeyed by these generated {ρ−f}histograms. In fact, at the end of each step in each of these *n* new runs, we recover an null-obeying {ρ−f}histogram pair. Of all these null-obeying {ρ−f}histograms, that which maximises the posterior (the pair ρ^*, f^* does, say) is recognised as our equivalent of θ^*. All the other histograms that we recover from runs of CHASSIS - performed with observed data - are compared to this ρ^*, f^*.

Let there be a total of N {ρ − f}histograms recovered from all possible runs of CHASSIS - performed with observed data or the $D_{CHASSIS}$ data sets. If the number of cases for which $\Pr(\{\rho, f\}|\{data\}) > \Pr(\rho^*, f^*)$, is M, we obtain our *ev* as $1 - M/N$ (Equation 4). Thus, we set:

$$\Pr(\{\rho, f\} \in T|\{data\}) = \frac{M}{N} \qquad (6)$$

In line with FBST, the null is rejected for "small" *ev*.

Unlike with *p*-values, this "small"ness can be objectively qualified in terms of minimisation of the loss function (Pereira, Stern & Wechsler 2008; Madruga, Esteves & Wechsler 2001).

4.3. Results from implementation of FBST

The implementation of FBST, as described above, is invoked to estimate if the assumption of isotropy should be rejected, in the two different tracer classes that we deal with.

The estimated *ev* for the different PNe runs are (approximately):

– PNe-RUN I: 0.61,
– PNe-RUN II: 0.58,
– PNe-RUN III: 0.62.

The *ev* values for the three GC runs are:

– GC-RUN I: 0.96,
– GC-RUN II: 0.96,
– GC-RUN III: 0.93.

The total mass density distribution obtained by using the measured kinematic data is compared to ρ^* in Figure 5.

The results of our test for the goodness of the assumption of isotropy, given the data are:

– assumption is more likely to be invalid for the phase space from which the PNe data are drawn than from which the GC data is drawn.
– isotropy is a good description of the phase space that the GC data in NGC 3379 are drawn from, as in M87 and M49, as reported by Côté et al. (2003) and Côté et al. (2001) respectively.
– the two tracer samples have been drawn from significantly distinct phase space distributions, i.e. *the phase space of NGC 3379 is marked by at least two distinct basins of attractions* or that NGC 3379 is bistable if not multi-stable.
– the most likely mass density distribution obtained from GC data, under isotropy, is consistent with density recovered by CHASSIS from GC-RUN II.
– the most likely gravitational mass density under isotropy falls significantly below density recovered by CHASSIS with PNe data from PNe-RUN II.

It merits mention that while an *ev* > 0.9 would support confidence in the assumption of isotropy, the *ev* ~0.6 is not small enough to suggest complete rebuttal of the assumption of isotropy by the PNe data. In fact, all we can objectively infer from our analysis is the comparative adherence of the two data sets, to the assumption of isotropy.
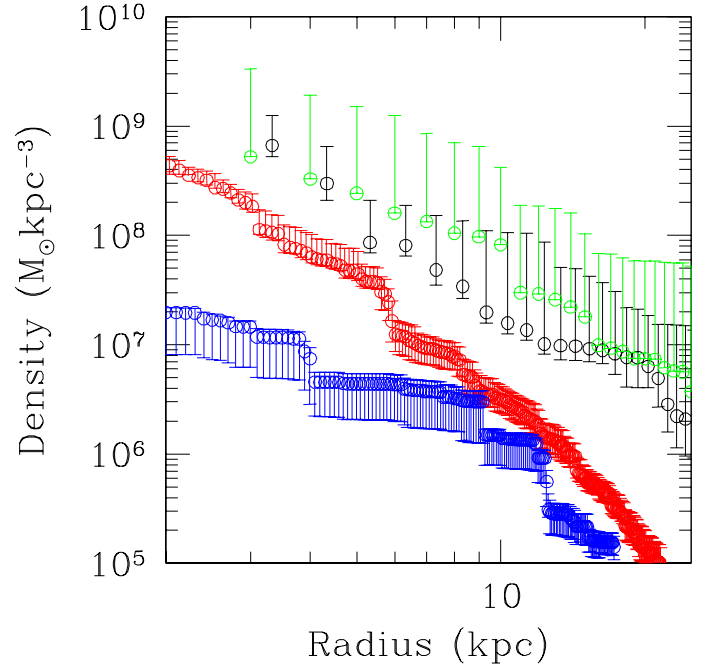
Fig. 5. The comparison between the density profile achieved upon convergence during a run of CHASSIS and the most likely density ρ^* that is recovered under the null hypothesis (implemented kinematic data are drawn from the isotropic phase space densities achieved at the end of runs GC-RUN II and PNe-RUN II). ρ from GC-RUN II is in black while ρ^* calculated from this run is in green; these density distributions are seen to be consistent within error bars. On the other hand, ρ and ρ^* from PNe-RUN II (in red and blue respectively) are significantly different.

4.3.1. Effect of Modeling Anisotropy with Isotropy-assuming CHASSIS

As was delineated in Chakrabarty & Portegies Zwart (2005), CHASSIS bears the peculiarity that at radii where phase space anisotropy prevails, the $\rho(r)$ recovered under the erroneous assumption of isotropy is an overestimation. This trend can be used to infer the state of isotropy in the true phase space from which the input kinematic samples are each drawn. Thus, we can explain the differences noted between the $\rho(r)$ recovered from PN2-RUN II and $\rho^*(r)$, if we attribute anisotropy to the phase space from which the PNe velocities are extracted. The overlap of $\rho(r)$ recovered from GC-RUN II and ρ^* indicates that the GC data is drawn from an isotropic phase space. In other words, the aforementioned peculiarity of CHASSIS supports the conjecture that NGC 3379 is a multi-stable system, unless the sampling of PNe and/or GC kinematic data are biased in some way.

At the same time, this peculiarity of CHASSIS implies that if full anisotropy were included in the analysis of the PNe data, the recovered density would no longer be overestimated, i.e. the recovered ρ would then be lower at most r, than that recovered from using the GC data. However, the full incorporation of anisotropy will not trigger much change in the ρ derived from the GC data. Thus, *accounting for anisotropy will enhance the difference between the density profiles obtained from the PNe and GC data sets*.

4.3.2. Distinct Mass Distributions

Though it is interesting to find that NGC 3379 is multi-stable, we are much more excited to note that the total mass density of NGC 3379 is recovered as distinct, when the two different data

sets are used. However, if we view the problem from the context of a Jeans equation formalism, we find that the effect of using two distinct $\sigma_p(r)$ and $v(r)$ profiles will in general imply distinct enclosed mass distributions $M(r)$. Again, within CHASSIS, we realize that the projection of a trial $f(E)$ into the space of observables (x_p, y_p, v_z), given a trial potential $\Phi(r)$, would yield distinct likelihood structures for distinct input kinematic data - the global maxima in the likelihood function ($\mathcal{L}$) would correspond to distinct $\{\rho - f\}$histogram pairs, i.e. each data set would in general imply distinct mass density distributions as solutions. Here the projection of $f(E)$ into the *pdf* of the space of observables is:

$$\mu(x_p, y_p, v_z) = \int f[E(v_x^2 + v_y^2 + v_z^2 + 2\Phi(r))]dv_x dv_y dz \qquad (7)$$

and $\mathcal{L} = \ln \sum \mu$. Here the summation is taken over the whole data set.

5. Discussions

Our results indicate that the mass distribution tracked by the PNe velocities is significantly less than that implied by the GC kinematics! Individual consideration of the PNe analysis leads to a "naked" interpretation for NGC 3379, in line with what was suggested by Douglas et. al (2007) and Romanowsky et. al (2003), though the $\Upsilon(< r)$ recovered from the PNe-RUN, at $5R_E$ (lying between 10 and 20) is slightly higher than what Douglas et. al (2007) advance, due to the assumption of isotropy in our work (which artificially augments $\rho(r)$ wherever anisotropy exists). The GCs on the other hand imply a dark matter rich system, with $\Upsilon_B(< r) \in [30, 80]$, at the 1-$\sigma$ error level, at about $9R_E$.

Alternative representations of the matter density in NGC 3379 corroborate the same dichotomous picture. These include:

- v_c calculated from the PNe runs concur with the Keplerian fall-off with r but that from the GC runs are significantly flatter (Figure 2).
- the $M(r)$ recovered from the PNe runs flatten by about $r=7$ kpc. On the other hand, the $M(r)$ recovered from the GC runs is rising even at 25 kpc (edge of the radial extent of the data).

We try to reconcile with the results by asking if we could have misinterpreted something.

5.1. Could We be Wrong?

Is it possible that the assumptions in our analysis have misled us to develop this seemingly dichotomous view of the galaxy? Or could there be a problem related to the collection of the data samples that is causing this view?

5.1.1. Ignoring Anisotropy in Analysis

Would the distinction noted in the $\rho(r)$ recovered with the PNe and GC runs, have vanished if we had not assumed velocity isotropy in our analysis? The answer is no, as explained below.

As discussed earlier in Section 4.3.1, *the inclusion of anisotropy will render the recovered $\rho(r)$ lower than the profile currently recovered by CHASSIS from PNe data*. In other words, inclusion of anisotropy will increase the gap between the density profiles recovered from the PNe and GC data. Thus, the only way to reconcile the difference between the density distributions recovered from the PNe runs and GC runs, is to suggest that the GC data are drawn from a phase space distribution that

is even more strongly anisotropic than the one from which the PNe data are drawn. However, our statistical testing indicates the exact opposite. This implies that there is no way we can reconcile the differences in the recovered density distributions, by incorporating velocity anisotropy.

5.1.2. Asphericity?

It has been argued that NGC 3379 is actually triaxial rather than spherical (Dekel et. al 2005); the point is that σ_p would then appear deflated for certain inclinations and that this is the reason for the PNS studies to recover spuriously low masses. (Romanowsky et. al 2003; Douglas et. al 2007). Douglas et. al (2007) reject this as improbable, based on the distribution of the intrinsic axial ratios of elliptical galaxies. However, this argument is unacceptable, owing to (i) the obvious errors involved in the constraining of a property of an individual system, knowing only a sample distribution of the characteristic and (ii) the essentially unconstrained nature of the sought distribution of the intrinsic axial ratios.

Within CHASSIS, the *assumption of sphericity involves the geometry of the sought gravitational potential of the system and not that of the tracer spatial distribution*. Also, CHASSIS does not employ the σ_p profile derived from observations, but measurements of individual tracer LOS velocities.

If however, the radially symmetric assumption on Φ is misplaced, then this will affect results - the greater the deviation from the assumption of $\Phi = \Phi(r)$, the greater is the expected difference in likelihood structure recovered from using the corresponding data. However, we have indeed checked for the validity of this assumption when we checked for the adherence of an observed data to the assumption of phase space isotropy. As explained above, the results of such a test indicate distinct mass density distributions.

5.1.3. GC Data?

It could be argued that the GCs used in our work do not really trace the mass of NGC 3379 but of a shared dark matter distribution that might pervade the inter-galaxy space between NGC 3379 and one or more of its neighbours, among which, NGC 3384 is the closest. But, it is precisely to avoid such a predicament that we use the velocities of only 30 of the GCs that Bergond et. al (2006) advance as definitely belonging to NGC 3379. Besides, interference from the dark halo of a neighbouring galaxy is not expected to explain the significant difference between the recovered $M(r)$ profiles, at 10 kpc. Such effects, if any could kick in at higher radii.

5.1.4. Non-linear Dynamics

It is perhaps likely that a fraction of the PNe and GC orbits are chaotic. Even if this were the case, this does not nullify the observation that the phase space distributions from which the PNe and GC data are drawn are different and that such data imply distinct mass distributions. If anything, the probabilistic measures of the free-form f and ρ that CHASSIS provides the best possible description of the ramifications of non-linearity.

5.2. Risk of using Tracer Kinematics

To sum up the arguments of Section 4.3.2, we state that in general, kinematic data drawn from distinct phase spaces will yield

distinct $M(r)$ profiles and this is not solely because of the issue of phase space isotropy. Thus, for example, within the Jeans equation formalism, it is possible to obtain distinct $M(r)$ using kinematics from two data sets that are drawn from two distinct phase space distributions that are equally anisotropic (as parameterised by the anisotropy parameter $\beta(r)$) - then $d\ln\sigma_p(r)/d\ln r$ and $d\ln\nu(r)/d\ln r$ terms would in general be different in the two cases, even if $\beta(r)$ is the same. In other words, it is not surprising that we think that we have inferred distinct mass density distributions for the same galaxy, using distinct tracer kinematic data.

To put it differently: it is potentially risky to refer to the gravitational potential recovered using an observed tracer sample, as the potential of the galaxy. We have demonstrated this with the example of NGC 3379 and shown that the distinct mass distributions recovered, cannot be made to collapse into consistent forms by invoking the effects of phase space anisotropy, non-linear effects or by attributing errors to the observed GC data.

However, in contrast to PNe and GC samples, if two sets of tracer kinematics can be inferred to have been drawn from the same phase space, we will expect consistency in the gravitational matter density that is recovered by using such data sets in a mass determination formalism. Such a possibility is discussed in the following section.

5.3. Distinct Phase Space Distributions & Multi-stability of NGC 3379

We have seen that in Section 4.3 that the *phase space of the galaxy NGC 3379 is actually marked by multiple attractors*. The stability of such a dynamical system is an interesting issue. It is possible that *such a configuration arises from the modification of the system, introduced by the action of resonant perturbations* (Chizhevsky, Corbalan & Pisarchik 1997)[2]. We conjecture that such is possible in NGC 3379. The original primary attractor is split into multiple new attractors, one of which could be that subset of the galactic phase space that can describe the GC orbital distribution while the other could explain the PNe orbits.

However, such distinct phase space density distributions is not altogether surprising, given that the evolutionary history of PNe and GCs is very different. PNe are basically the end states of (low to medium mass) stars. Thus, it is envisaged that the phase space density that describes PNe motion will be similar to that of old, low to medium mass stars. In that case, PNe velocity data and the kinematics of such a stellar population will be drawn from the same part of the galactic phase space and the recovered $M(r)$ will be consistent in these two cases.

5.4. "Naked Galaxies"

The upshot is that the splitting of the entire orbital distribution into two or more distinct basins of attractions, is not improbable. When such occurs, it is possible to fall prey to our ignorance about the galactic phase space structure, and infer spurious galactic properties based on the characteristics of one of these distinct regions of phase space. Expectedly, increasing the range of measurements to multiple tracer classes, will only help to impose tighter constraints on the solution.

It is possible, that the low DM content of the 5 "naked" galaxies, (Romanowsky et. al 2003) was achieved as a result

of this situation. Incorrect mass distributions can emanate from substituting information about the galactic phase space by that of orbital distribution of the particular class of tracers at hand. Scanning over a wide range of the parameterisation of velocity anisotropy, is not enough in general, to compensate for the errors caused by this substitution. Thus, cross-validation of results obtained with different tracer classes, wherever possible, is welcome.

5.5. True Mass Distribution

At the end of the analyses and conjectures presented above, we will naturally want to know what the true mass distribution of NGC 3379 is. Given the greater adherence to the assumption of isotropy, the results from the GC runs should be considered as better approximations of the state of NGC 3379 than those from the PNe runs.

Thus, NGC 3379 is advanced as a dark matter rich galaxy, with $\Upsilon_B(< r) \in [30, 80]$, approximately, at a radius just inner to 20 kpc ($r \approx 9R_{eff}$), where this range of values pertain to 1-σ errors of analysis. The enclosed mass at this radius is about $5^5_{2.5}\times10^{11}M_\odot$. The LOS velocity dispersion is flat, as is typical of dark matter rich systems. Enhancement of the GC data sample will reduce these errors of analysis.

We conclude that it is risky to refer to the mass distribution recovered upon application of tracer kinematics, as the mass distribution of the galaxy.

References

Banerjee, P., 2003, *Nonlinear Optics Theory, Numerical Modeling and Applications*, Marcel Dekker Inc., New York, Basel.

Basu, D., 1975, *Sankhya A*, 37, 1.

Bergond, G., Zepf, S. E., Romanowsky, A. J., Sharples, R. M., & Rhode, K. L., 2006, A&A, 448, 155.

Birnbaum, A., 1962, *Jl. of the American Statistical Association*, 57, 269.

Chakrabarty, D., 2009, *Proceedings of the 18th IMACS World Congress MODSIM 2009, Cairns*, arXiv:0905.2524.

Chakrabarty, D. & Raychowdhury, S., 2008, AJ, 135, 2350.

Chakrabarty, D. & Ferrarese, L., 2008, *International Journal of Modern Physics D, as part of proceedings for the 6th International Workshop on Data Analysis in Astronomy, "Modelling and Simulations in Science"*, Vol 17, No 2.

Chakrabarty, D., 2006, ApJ, 131, 2561.

Chakrabarty, D., & Portegies Zwart, S., 2004, ApJ, 128, 1046.

Chakrabarty, D., & Saha, P., 2001, ApJ, 122, 232.

Chizhevsky, V. N., Corbalan R., & Pisarchik, A. N., 1997, *Physical Review E*, 56, 1580.

Côté, P., McLaughlin, D. E., Cohen, J. G., & Blakeslee, J. P., 2003, ApJ, 591, 850.

Côté, P., McLaughlin, D. E., Hanes, D. A., Bridges, T. J., Geisler, D., Merritt, D., Hesser, J. E., Harris, G. L. H., Lee, M. G., 2001, ApJ, 559, 828.

Dekel, A., Stoehr, F., Mamon, G. A., Cox, T. J., Novak, G. S., & Primack, J. R., 2005, Nature, 437, 707.

Douglas, N. G., Napolitano, N. R., Romanowsky, A. J., Coccato, L., Kuijken, K., Merrifield, M. R., Arnaboldi, M., Gerhard, O., Freeman, K. C., Merrett, H. R., Noordermeer, E. & Capaccioli, M., 2007, ApJ, 664, 257.

Douglas, N. G., Arnaboldi, M., Freeman, K. C., Kuijken, K., Merrifield, M. R., Romanowsky, A. J., Taylor, K., Capaccioli, M., Axelrod, T., Gilmozzi, R.,

---

[2] In this work it was shown that such weak periodic perturbations induce two or more attractors in the system in place of the one initial attractor. Thus, the system is rendered *bistable* (Ott 1993; Banerjee 2003).

Hart, J., Bloxham, G. & Jones, D., 2002, *The Publications of the Astronomical Society of the Pacific*, 114, 1234.

Hastings, W. K., 1970, *Biometrika*, 57, 97.

Hubbard, R. & Lindsay, M. R., 2008, *Theory & Psychology*, 18, 69.

Kempthorne, O. & Folks, L., 1971, *Probability, Statistics and Data Analysis*, Ames, I0: Univ. of Iowa Press.

Koopmans, L. V. E., 2006, EAS Publications Series, 20, 161.

Łokas, E. L., & Mamon, G. A. 2003, MNRAS, 343, 401.

Madruga, R. M., Luis E. G. & Wechsler, S., 2001, *Test*, 10, 291.

Ott, E., 1993, *Chaos in Dynamical Systems*, Cambridge University Press, Cambridge, UK.

Pellegrini, S., & Ciotti, L. 2006, MNRAS, 370, 1797.

Pereira, C. A. de B., Stern, J. M. & Wechsler, S., 2008, *Bayesian Analysis*, 3, 79.

Pereira, C. A. & Stern, J. M., 1999, *Entropy*, 1, 99.

Romanowsky, A. J., Douglas, N. G., Arnaboldi, M., Kuijken, K., Merrifield, M. R., Napolitano, N. R., Capaccioli, M., & Freeman, K. C., 2003, *Science*, 301, 1696.

Sambhus, N., Gerhard, O., & Méndez, R. H., 2006, AJ, 131, 837.

Sambhus, N., Gerhard, O., & Méndez, R. H., 2005, Planetary Nebulae as Astronomical Tools, 804, 317.

Sawyer Hogg, H., 1947, Journal of the Royal Astronomical Society of Canada, 41, 265.